Chemical Science

ROYAL SOCIETY OF CHEMISTRY

EDGE ARTICLE

View Article Online
View Journal | View Issue

Cite this: *Chem. Sci.*, 2024, **15**, 16125

All publication charges for this article have been paid for by the Royal Society of Chemistry

Received 8th July 2024
Accepted 5th September 2024

DOI: 10.1039/d4sc04519j

rsc.li/chemical-science

Ambient catalyst-free oxidation reactions of aromatic amines using water radical cations†

Xiaoping Zhang, *[a] Pinghua Hu,[a] Minmin Duan,[a] Konstantin Chingin, [b] Roman Balabin, [b] Xinglei Zhang*[a] and Huanwen Chen*[b]

Water radical cations play a pivotal role in various scientific and industrial fields due to their unique reactivity and capacity to drive complex chemical transformations. Here we explored the formation of quaternary ammonium cations through the direct oxidation reaction of aromatic amines, facilitated by water radical cations within water microdroplets. This process was monitored *via in situ* mass spectrometry and occurs under ambient conditions, negating the need for traditional chemical catalysts or oxidants and achieving an impressive yield of approximately 80%. Additionally, we employed a multi-channel spray system and enhanced both the reactant concentration and flow rate, thereby enabling gram-scale synthesis. These findings not only demonstrate the effectiveness and eco-friendliness of microdroplet chemistry but also provide a new understanding of heterogeneous $^{\bullet}OH$ generation channels, thereby boosting the synthetic efficiency and sustainability of chemical processes.

Introduction

The oxidation of organic compounds is an essential reaction widely studied in academia as well as in the chemical industry.[1,2] Despite numerous research efforts, the selective oxidation of organic substrates remains a critical challenge. It would be of great value to be able to hydroxylate aromatic amines in a regio-controlled manner under mild conditions, using inexpensive oxidants and avoiding the use of transition metals, thereby preparing synthetically significant structures.[3] There are few reported strategies for the synthesis of amine *N*-oxides[4,5] and quaternary ammonium cations.[6,7] Quaternization, forming the quaternary ammonium cation, prevents inversion and locks the configuration of the nitrogen stereocenter. The synthesis of quaternary ammonium compounds is of great significance for drug development. Therefore, developing a general strategy for constructing quaternary ammonium compounds has always been a major challenge in synthetic chemistry.

Mass spectrometry (MS) has been widely applied to the study of chemical reactions in recent years, enabling the *in situ* capture of short-lived intermediates during reactions.[8–10] In particular, the emergence of microdroplet chemistry in MS has garnered much attention due to the "catalytic" role of the interface in accelerating reactions, making it a unique platform for investigating and conducting chemical reactions.[11–13] Recently, it has been discovered that simple water microdroplets can significantly accelerate the rate of organic reactions.[14,15] For instance, Lee *et al.* reported spontaneous oxidation and reduction reactions in microdroplets without the addition of reducing or oxidizing agents, where the reactive species involved are the hydroxyl radical and hydrogen peroxide.[16] Gong *et al.* hypothesized that electrons at the microdroplets' air–water interface are responsible for the reduction of ethyl viologen.[17] Cooks and colleagues suggested that water radical cations, generated in organic-solvent microdroplets containing trace amounts of water, play a key role in the oxidation of aromatic sulfones to sulfonic acids.[18,19] Our group has also demonstrated the strong reactivity of $(H_2O)_2^{+\bullet}$, which can transform C=C bonds into epoxides[20,21] and C=O bonds to generate $[M + H_2O]^{+\bullet}$.[22] Most recently, we discovered that $(H_2O)_2^{+\bullet}$ can even convert nitrogen (N_2), a highly inert molecule, into NH_2OH and HNO.[23] The diverse chemistry of $(H_2O)_2^{+\bullet}$ has been attributed to the co-existence of two distinct structures: $[H_3O^+\cdots{}^{\bullet}OH]$ and $[H_2O\cdots OH_2]^{+\bullet}$,[24] which can exhibit the properties of $^{\bullet}OH$, H_3O^+, and $H_2O^{+\bullet}$.

The electrochemical oxidation of *N*,*N*-dimethylaniline and its derivatives has been studied extensively.[25,26] A common feature in all cases is that the oxidation of aniline begins with the nitrogen atom losing one electron to yield the radical cation.[25,26] From this point, the oxidation mechanism varies depending on the level of substitution at the nitrogen atom and the basicity of the reaction medium. Yoshida and co-workers reported a highly chemoselective metal-free method for the aryl C–H amination of aromatic compounds with pyridine and

[a]*Jiangxi Key Laboratory for Mass Spectrometry and Instrumentation, East China University of Technology, Nanchang, 330013, P. R. China. E-mail: zhangxpsunshine@163.com; leizi8586@126.com*

[b]*School of Pharmacy, Jiangxi University of Chinese Medicine, Nanchang 330004, P. R. China. E-mail: chw8868@gmail.com*

† Electronic supplementary information (ESI) available. See DOI: https://doi.org/10.1039/d4sc04519j

imidazole, resulting in the formation of *N*-arylpyridinium and *N*-arylimidazolium ions, respectively, through electrochemical oxidation.[27,28] Functional groups such as N–O bonds are crucial for biological functions. In this work, we report the synthesis of quaternary ammonium cations through the direct *N*-hydroxylation of aromatic amine in water microdroplets, notably without the need for applying an additional external voltage to the sample solution. The quaternary ammonium product was characterized by MS and nuclear magnetic resonance (NMR) experiments, demonstrating good universality in the reaction.

Experimental procedures

Chemicals and materials

D_2O was purchased from Cambridge Isotope Laboratories, Inc. (Andover, MA, USA). Ultra-purity Ar (>99.999%) and ultra-purity helium (>99.999%) were obtained from Jiangxi Guoteng Gas Co. Ltd (Nanchang, China). *N*,*N*-Dimethylaniline (DMA, **1**), 4-methoxyl-*N*,*N*-dimethylaniline (4-MeO-DMA, **2**), 4-methyl-*N*,*N*-dimethylaniline (4-Me-DMA, **3**), 4-chloro-*N*,*N*-dimethylaniline (4-Cl-DMA, **4**), 4-bromo-*N*,*N*-dimethylaniline (4-Br-DMA, **5**), *N*,*N*-diethylaniline (DTA, **6**), 3-hydroxy-*N*,*N*-dimethylaniline (3-OH-DMA, **7**), 2-hydroxy-*N*,*N*-dimethylaniline (2-OH-DMA), and 4-hydroxy-*N*,*N*-dimethylaniline (4-OH-DMA) were purchased from Shanghai Sun Chemical Technology Co., Ltd (China), each with a purity of over 99%. *N*,*N*-Dimethylaniline *N*-oxide was purchased from Shanghai Laibo Chemical Technology Co., Ltd (China), also with a purity exceeding 99%. Water used in all experiments was purified using a Milli-Q system (Millipore, USA).

Experimental setup

The experimental setup to study the *N*-hydroxylation reaction between DMA and $(H_2O)_2^{+\bullet}$ in water microdroplets is depicted in Fig. 1a. Argon gas was introduced at a flow rate between 0.3 and 1.0 MPa. The produced H_2O/DMA solution was directed to a fused silica capillary situated inside a larger capillary through which argon gas flows at high pressure. The distance from the inlet of the mass spectrometer capillary to the tip of the ion source ranged from 5 to 20 mm.

MS settings

MS detection was performed using an LTQ-XL ion trap mass spectrometer (LTQ-XL, Thermo Scientific, San Jose, CA, USA). The temperature of the ion transfer capillary was set at 250 °C. The capillary voltage was 20 V, and the tube lens voltage was set at 30.0 V. The pressure in the ion trap was maintained at 1×10^{-5} torr. High-purity helium (99.999%) was used as the collision gas. Collision-induced dissociation (CID)-MS experiments were conducted by applying an alternating current excitation voltage to the end caps of the ion trap to induce collisions of the isolated ions. CID-MS spectra were obtained by activating the precursor ions at a normalized collision energy ranging from 0% to 50%. Ion detection was conducted in the positive ion mode. Other LTQ-XL parameters were automatically optimized by the system.

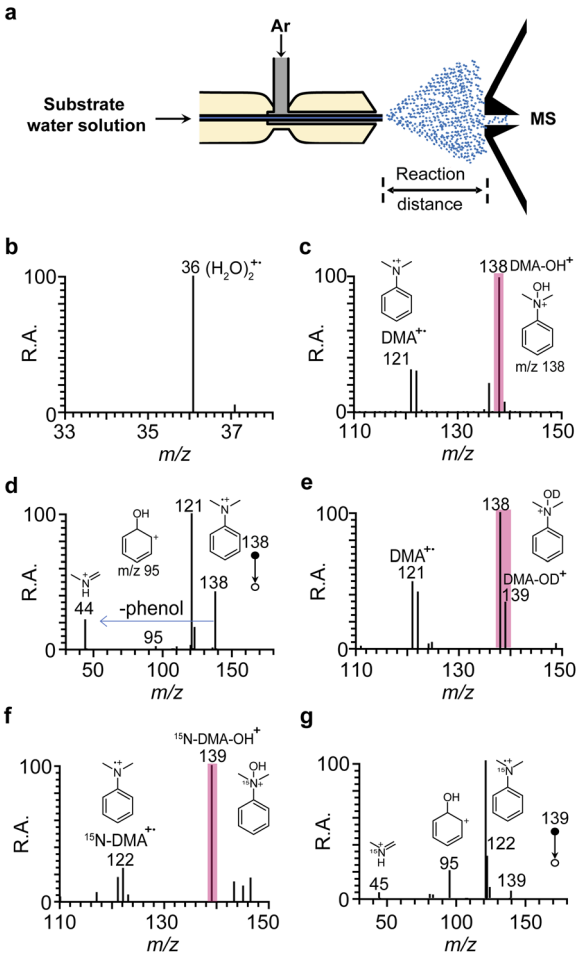

Fig. 1 Mass spectrometric analysis of the spontaneous hydroxylation reaction between DMA and $(H_2O)_2^{+\bullet}$ in water microdroplets. (a) A schematic drawing of the experimental setup. (b) A typical mass spectrum showing the generation of $(H_2O)_2^{+\bullet}$ at *m*/*z* 36 when spraying pure water. (c) A typical mass spectrum demonstrating the spontaneous generation of $DMA^{+\bullet}$ at *m*/*z* 121 and $DMA{-}OH^+$ at *m*/*z* 138 when spraying a DMA–water solution. (d) A tandem mass spectrum of the product ion at *m*/*z* 138. (e) A typical mass spectrum illustrating the spontaneous generation of $DMA^{+\bullet}$ at *m*/*z* 121 and the $DMA{-}OD^+$ product at *m*/*z* 139 when spraying a D_2O solution with DMA. (f) A typical mass spectrum illustrating the spontaneous generation of ^{15}N-$DMA^{+\bullet}$ at *m*/*z* 122 and the ^{15}N-$DMA{-}OH^+$ product at *m*/*z* 139 when spraying ^{15}N-DMA solution. (g) A tandem mass spectrum of the product ion at *m*/*z* 139 in Fig. 1f. DMA : *N*,*N*-dimethylaniline.

High-resolution MS experiments were conducted using an Orbitrap-XL mass spectrometer (Thermo Scientific, San Jose, CA, USA) equipped with a homemade ESI setup. The instrument operated at a resolution of up to 300 000. Mass spectra were averaged over 30 scans during a sampling period of 0.5 minutes, covering a mass-to-charge (*m*/*z*) range of 15 to 200. Other Orbitrap-XL parameters were consistent with the LTQ-XL parameters previously mentioned.

Yield calculation

The method for yield calculation in this work was derived from the rough estimates of the yields of microdroplet synthesis reactions reported by the Cooks group and Zare group.[29,30] This

was obtained by measuring the conversion ratio: the ratio of the intensity of the product (P) to the sum of the intensities of the reactant (R) and product (P), *e.g.*, [P]/([R] + [P]).

Scale-up experiments

Synthesis of DMA–OH was carried out through the scale-up microdroplet reaction of DMA aqueous solution. First, a capillary tube with an inner diameter of 150 μm was placed in a nebulizer with an argon pressure of 0.4 MPa. A DMA aqueous solution with a concentration of 1000 μg mL^{-1} was placed in a syringe and pumped into the capillary tube at a rate of 20 μL min^{-1} to form microdroplets. These droplets were sprayed into a three-necked flask with a condenser (Fig. S1a†). An electrode was placed at one end of the flask to neutralize excess positive charge, while the other end was vented. In the venting section, ethyl acetate was used to absorb the product that may be contained in the carrier gas. The droplets were collected continuously for 10 h, combined with the contents of the flask and ethyl acetate absorption solution, and then evaporated to obtain yellow oil crude products. The crude product was further purified by thin layer chromatography using petroleum ether and ethyl acetate as eluents. The purified target product was obtained and characterized by MS and NMR.

Synthesis of ^{15}N-labeled DMA

An efficient synthesis of ^{15}N-labeled DMA, based on ref. 31, was conducted using $^{15}NH_4Cl$ and benzoyl chloride as starting materials. The synthesis involves the following steps: first, $^{15}NH_4Cl$ was reacted with benzoyl chloride to provide ^{15}N-benzamide. Next, ^{15}N-benzamide underwent Hofmann degradation to produce ^{15}N-aniline. Finally, ^{15}N-aniline was methylated using methyl 4-methylbenzenesulfonate to form ^{15}N-DMA. The product, ^{15}N-DMA, was also subjected to a scale-up experiment to confirm the structure of the hydroxylation product of DMA.

Density functional theory (DFT) calculations

Theoretical calculations were performed using the Dmol3 software package based on the linear combination of atomic orbitals method. Electron–ion interactions were described using all electron potentials. A double numerical polarized (DNP) basis set was employed to expand the wave functions with an orbital cutoff of 3.7 Å. For the electron–electron exchange and correlation interactions, the B3LYP functional was used throughout. The van der Waals interaction was described using the DFT-D2 method proposed by Grimme. During the geometry optimizations, all the atoms were allowed to relax. In this work, the convergence criterion for the electronic self-consistent field (SCF) loop was set to 10^{-6}. The atomic structures were optimized until the residual forces were below 0.002 Ha $Å^{-1}$.

Results and discussion

Hydroxyl quaternization of DMA

Fig. 1a illustrates the experimental setup for the microdroplet reaction. Briefly, substrate water solutions are propelled through a fused silica capillary using a syringe pump; this capillary is nested within a larger coaxial capillary through which high-pressure argon sheath gas flows. Fig. 1b presents a typical mass spectrum that demonstrates the spontaneous generation of the water dimer radical cation $(H_2O)_2^{+\bullet}$ at *m*/*z* 36 when pure water is sprayed to form microdroplets, a phenomenon also reported by Xing *et al.*[32] They observed the presence of $(H_2O)_2^{+\bullet}$ at the air–liquid interface, which is essentially [$^{\bullet}OH\cdots H_3O^+$], where a hydroxyl radical is combined with a hydronium cation *via* hydrogen bonding. Our group has also reported the generation of $(H_2O)_2^{+\bullet}$ using energy-tunable corona discharge ionization mass spectrometry, demonstrating its excellent reactivity.[33] One form of $(H_2O)_2^{+\bullet}$ (*m*/*z* 36), [$^{\bullet}OH\cdots H_3O^+$], acts as a carrier of the hydroxyl radical, facilitating numerous reactions.[33,34]

Initially, we explored the idea of extracting electrons from the substrates and further hydroxylation using microdroplets, selecting DMA (**1**) for mechanistic studies and optimization of reaction conditions. Fig. 1c displays a typical mass spectrum, highlighting the observation of the spontaneous hydroxylation product at *m*/*z* 138 (base peak) when spraying a DMA–water solution, which indicates that the reaction of DMA with $^{\bullet}OH$ in $(H_2O)_2^{+\bullet}$ may occur. Parent $DMA^{+\bullet}$ radical cations are also present but with lower intensity. High-resolution mass spectrum data revealed a peak for $DMA^{+\bullet}$ + $^{\bullet}OH$ at *m*/*z* 138.09104 (error of −2.1 ppm), further confirming the hydroxylation product of DMA (Fig. S2†). The tandem MS spectrum of the hydroxylation product (*m*/*z* 138) yielded fragment ions at *m*/*z* 121, *m*/*z* 95 and *m*/*z* 44 (Fig. 1d), corresponding to the loss of $^{\bullet}OH$, $CH_3N{=}CH_2$, and phenol, respectively, consistent with its structural assignment (Fig. S3†). However, it remains uncertain whether the $^{\bullet}OH$ is attached to the *ortho*- or *para*-position to form a phenol structure or connected to the nitrogen atom of DMA to form a quaternary ammonium structure.

To further determine the position of the $^{\bullet}OH$ interaction with the DMA structure at *m*/*z* 138, tandem MS experiments for isomers *N*,*N*-dimethylaniline *N*-oxide, 2-OH-DMA, 3-OH-DMA, and 4-OH-DMA standards were conducted. The tandem MS spectrum of protonated *N*,*N*-dimethylaniline *N*-oxide displayed the same fragment ions at *m*/*z* 44, *m*/*z* 95 and *m*/*z* 121 (Fig. S4†) as those observed in the tandem MS spectrum of *m*/*z* 138 generated by the spraying of DMA solution, with consistent intensities. However, the tandem MS spectra of protonated 2-OH-DMA, protonated 3-OH-DMA, and protonated 4-OH-DMA showed major fragmentation ions at *m*/*z* 123, which differed from those of *m*/*z* 138 generated by spraying the DMA solution (Fig. S5†). These results confirmed that the structure of *m*/*z* 138 obtained from spraying of DMA solution corresponds to *N*-hydroxyl-*N*,*N*-dimethylanilinium, a quaternary ammonium structure. It was reported that *N*,*N*-dimethylaniline *N*-oxide and *N*-hydroxyl-*N*,*N*-dimethylanilinium can easily interconvert.[5] Thus, the product at *m*/*z* 138 generated by the spraying of DMA solution is *N*-hydroxyl-*N*,*N*-dimethylanilinium. The formation process of fragment ions at *m*/*z* 121, *m*/*z* 95 and *m*/*z* 44 from the dissociation of protonated *N*,*N*-dimethylaniline *N*-oxide is clearly described in detail (Fig. S3†), and involves the OH

transfer reaction. This is similar to the reactions reported in previous studies.[35]

When isotope-labeled D_2O or ^{15}N-DMA was used in the experiments, the corresponding deuterium labeled ions at *m*/*z* 139 (Fig. 1e) and ^{15}N-labeled ions at *m*/*z* 139 (Fig. 1f) were both clearly observed. The dissociation of the *m*/*z* 139 ions from D_2O and ^{15}N-DMA displayed similar fragmentation patterns to those of *m*/*z* 138, with characteristic fragment ions at *m*/*z* 44, *m*/*z* 96, and *m*/*z* 121 (Fig. S6† and 1g). Consequently, the results of high-resolution MS experiments, tandem MS experiments of different standards for OH-DMA isomers, and isotope-labeling experiments all supported the hypothesis that the ion generated at *m*/*z* 138 is a quaternary structure known as *N*-hydroxyl-*N*,*N*-dimethylanilinium during the spraying of the DMA–water solution. This indicates that a large amount of quaternization products can obtained simply by spraying of the DMA–water solution.

We conducted additional experiments using methanol, acetonitrile, and their mixed solutions with water to determine if similar phenomena and products could be observed. The effects of different solvents on the intensity of hydroxylation products are shown in Fig. S7.† Our results showed that no hydroxylation products were detected in methanol and acetonitrile solvents (Fig. S7†). However, hydroxylation products were observed in their mixed solutions with water, with the highest intensity observed when pure water was used as the solvent (Fig. S7†). This indicates that water plays a crucial role in promoting the reaction, likely due to its ability to facilitate the formation of water radical cations, which subsequently lead to hydroxylation products.

Optimization of conditions for hydroxylation of DMA

DMA was chosen as the model substrate for optimizing reaction conditions. We explored the experimental conditions affecting the yields of *N*-hydroxylation of DMA and found that gas pressure was a significant factor (Fig. 2a). Higher gas pressure facilitates the formation of smaller droplets, enhancing the electric field intensity on the surface of the droplets. This finding is consistent with a previous report by Xing *et al.*[32] When the strength of the electric field exceeds the oxidation potential of the substrate, an electron is extracted from the substrate. However, when the argon pressure is increased beyond a certain point, the pressure at the spray outlet drops sharply. This disturbance affects the surrounding airflow, preventing the target substance from entering the mass spectrometer efficiently and resulting in decreased yields of the product ions.

We also examined the effects of the concentration of the aqueous DMA solution, the flow rate of the aqueous DMA solution, and the distance between the tip of the capillary tube and the MS inlet on the hydroxylation reaction. For the reaction distance, a noticeable increase in the yields of products at *m*/*z* 138 was observed as the distance increased from 1 to 6 cm (Fig. 2b), indicating that the reaction occurred within the microdroplets rather than in the gas phase inside the mass spectrometer. Similarly, when the sample flow rate was optimized to 8 μL min^{-1} (Fig. 2c), the products exhibited the highest

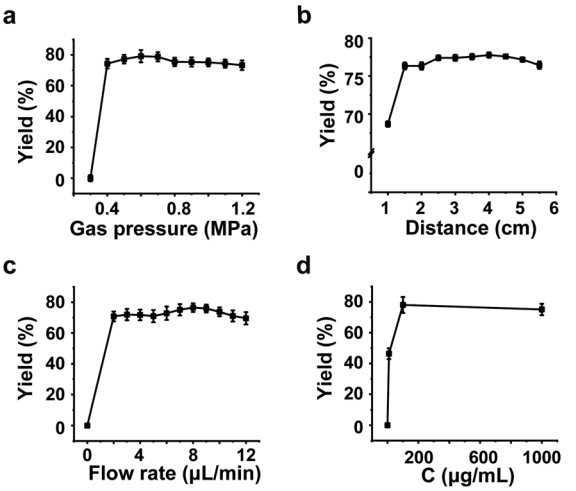

Fig. 2 Effects of microdroplet working conditions on the yields of hydroxylation products of *N*,*N*-dimethylaniline (DMA) at *m*/*z* 138. (a) Yields as a function of gas pressure. (b) Yields as a function of the distance between the tip of the capillary tube and the MS inlet. (c) Yields as a function of the flow rate of the aqueous DMA solution. (d) Yields as a function of the concentration of the aqueous DMA solution. *C*: concentration.

yield. This may be because, at a fixed pressure, excessively increasing the flow rate results in the formation of larger droplets or even incomplete nebulization, thereby reducing the target ion signal. The yields of the products increased with the sample concentration and eventually stabilized (Fig. 2d). Considering that excessive sample concentration could impact the mass spectrometer, 100 μg mL^{-1} was ultimately selected for subsequent experiments.

Substrate scope for hydroxyl quaternization

Next, we evaluated the substrate scope for relatively electron-rich aromatics, encouraged by the accelerated hydroxylation of DMA in the water microdroplet. Hydroxylation reactions were found to be compatible with various 4-substituted functional groups on DMA, such as electron-donating groups like –OCH_3 (4-MeO-DMA, **2**) and –CH_3 (4-Me-DMA, **3**), as well as electron-withdrawing groups like –Cl (4-Cl-DMA, **4**) and –Br (4-Br-DMA, **5**). Other diverse functional compounds tested included DTA (**6**) and 3-OH-DMA (**7**). In addition to the reaction studied between DMA and $^{\bullet}$OH in water microdroplets shown in Fig. 1, we investigated six other hydroxylation reaction systems involving 4-MeO-DMA, 4-Me-DMA, 4-Cl-DMA, 4-Br-DMA, 3-OH-DMA, and DTA. Mass spectra supported the occurrence of these reactions (Fig. 3). Hydroxylation reaction products with different functional compounds—3-OH-DMA (*m*/*z* 154 in Fig. 3a), 4-Me-DMA (*m*/*z* 152 in Fig. 3b), 4-MeO-DMA (*m*/*z* 168 in Fig. 3c), DTA (*m*/*z* 166 in Fig. 3d), 4-Cl-DMA (*m*/*z* 172 in Fig. 3e), and 4-Br-DMA (*m*/*z* 216 in Fig. 3f)—were clearly observed in the corresponding mass spectra. Generally, electron-donating groups facilitate the formation of *N*-hydroxyl quaternary amine ions, while electron-drawing groups are slightly less effective, possibly because electron-donating groups help

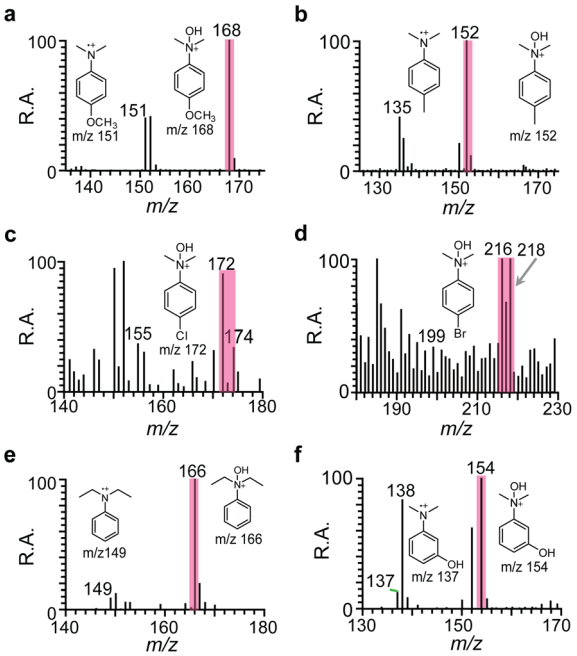

Fig. 3 Reaction scope of the *N*-hydroxylation reaction of DMA derivatives in water microdroplets. (a) 4-Methoxyl-*N*,*N*-dimethylaniline. (b) 4-Methyl-*N*,*N*-dimethylaniline. (c) 4-Chloro-*N*,*N*-dimethylaniline. (d) 4-Bromo-*N*,*N*-dimethylaniline. (e) *N*,*N*-Diethylaniline. (f) 3-Hydroxy-*N*,*N*-dimethylaniline.

disperse the positive charge and increase the electron density on the nitrogen atom, resulting in more stable compounds. When the $-CH_3$ group on the nitrogen atom was replaced by $-C_2H_5$, the *N*-hydroxyl quaternary amine ions were also efficiently produced. The corresponding *N*-hydroxylation products have been further elucidated using tandem MS spectra (Fig. S8†), which show similar cleavage patterns to those of the *N*-hydroxylation of DMA.

Our results demonstrated that these six different reactions are all spontaneous and ultrafast in microdroplets, compared to similar reactions facilitated by undivided electrochemical cells or strong oxidants.[5] Notably, the radical cations of 4-OMe-DMA, 4-Me-DMA, 4-Cl-DMA, 4-Br-DMA, 3-OH-DMA, and DEA were all observed in the mass spectra; however, the intensity of the radial cations varied, which might be a result of the differing oxidation potentials of these functional compounds. Therefore, the reactions in water microdroplets are characterized as radical/radical coupling. A yield of up to 80% for DMA hydroxylation reactions was calculated as the ratio of product intensity to the sum of reactant and product intensities, a method commonly used in MS-based micro-synthetic studies.[29,30,36] This relatively high product yield could be attributed to a relatively faster reaction rate of radical/radical coupling reactions. Our method showed very high yields for *N*,*N*-dimethylaniline compounds, which have low oxidation potentials. However, it resulted in low yields (<2%) for other alkylamines and piperidines, which have higher oxidation potentials (Fig. S9†). This indicates the limitations of our method when applied to these types of amines.

Scale-up reaction

To demonstrate the feasibility of our strategy for preparative synthesis, a scale-up reaction was performed. We modified the microdroplet reaction platform by extending the capillary into an electrically grounded collection vial (Fig. S1†). This vial contained a grounded device to provide favorable ion soft landing conditions. A DMA solution was used as the substrate, aiming to collect quaternary ammonium cations. The product yield for the DMA hydroxylation reaction was 90%, with approximately 10 mg collected over a 10 hour period using a concentration of 1 mg mL^{-1} and a flow rate of 20 μL min^{-1}. This yield is higher than the 80% yield reported from MS analysis, further confirming the reliability and reproducibility of our maximum yield. Additionally, by employing a four-channel spray system simultaneously (Fig. S1b†), with a concentration of 10 mg mL^{-1} and a flow rate of 100 μL min^{-1}, gram-scale synthesis (0.8 g) can be achieved. The method was also independently replicated in the laboratory of Jiangxi University of Traditional Chinese Medicine, where other researchers achieved consistent results, underscoring the robustness and reproducibility of our method. The formation of quaternary ammonium cations was further verified by ^{13}C-NMR spectroscopy, ^{1}H-NMR spectroscopy, and MS experiments. The ^{13}C-NMR spectrum and H-NMR spectrum recorded after the scale-up spraying of DMA experiments are shown in Fig. S10 and S11,† respectively. The signal at 68 ppm is assigned to the methyl group of *N*-hydroxyl-*N*,*N*-dimethylanilinium. This assignment was confirmed by comparing it with the ^{13}C-NMR and ^{1}H-NMR spectra of the corresponding *N*-oxide standard (Fig. S12 and S13†), where the signal at 63 ppm is assigned to the methyl groups. In addition, ^{15}N-DMA was synthesized and analyzed using ^{1}H-NMR and ^{13}C-NMR analysis (Fig. S14 and S15†). A scale-up microdroplet reaction of ^{15}N-DMA was then conducted, and the subsequent ^{1}H-NMR and ^{13}C-NMR analysis of the reaction products confirmed the hydroxylation on the nitrogen atom (Fig. S16 and S17†). These isotopically labeled experiments provided clear evidence of the hydroxylation process and the precise position of the hydroxyl groups.

Elucidation of the hydroxylation mechanism

With the successful detection of $DMA^{+\bullet}$ and its corresponding hydroxylated product, *N*-hydroxyl-*N*,*N*-dimethylanilinium, we advanced our investigation into the mechanism of the $DMA^{+\bullet}$ hydroxylation reaction. The reaction is crucial for transforming DMA into valuable pharmaceuticals and synthetic intermediates. Direct hydroxylation of hydrocarbon bonds in aromatic compounds is a straightforward and desirable method, but it remains challenging, especially from a sustainability perspective.[2] Cheng *et al.* described the dimerization process between two $DMA^{+\bullet}$ molecules through a radical cation–radical cation coupling mechanism.[37] The aqueous microdroplet environment can generate highly reactive species, including water radical cations and hydroxyl radicals.[25,32] The high surface area-to-volume ratio and the unique electric field effects at the microdroplet interface can facilitate the formation of these reactive species. In our system, the interaction of DMA with $(H_2O)_2^{+\bullet}$,

which is produced *in situ* within the microdroplets, leads to the oxidation of DMA to $DMA^{+\bullet}$. The $(H_2O)_2^{+\bullet}$ acts as a strong oxidant, abstracting an electron from DMA and resulting in the formation of the DMA radical cation. As previously discussed, the proposed mechanism for the formation of *m*/*z* 138 when spraying DMA solution in microdroplets may involve the reaction of $DMA^{+\bullet}$ with $^{\bullet}OH$ from the water dimer radical cation, which has the $[^{\bullet}OH\cdots H_3O^+]$ structure. Theoretically, as the radical cation is very unstable, it could couple with either another radical cation or with a neutral radical, with the latter pathway being more energetically favored. This is because the former process involves unfavorable charge–charge repulsion between two radical cations. We hypothesize that MS could elucidate the true reaction mechanism, as it allows us to capture and detect the radical cation of DMA and its derivatives, as shown in Fig. 3. Furthermore, control experiments reveal that the extracted ion chromatogram data show an increase in ion intensity of the peak at *m*/*z* 138 after spraying DMA samples, while the intensity of the peak at *m*/*z* 36 noticeably decreases (Fig. 4a). This observation suggests that the signals at *m*/*z* 138 are produced by the hydroxylation reaction between $DMA^{+\bullet}$ and $(H_2O)_2^{+\bullet}$.

A recent study indicates that at the water–oil interface, water dimers exist predominantly as H_2O^+–H_2O^- couples, with a preference for the negative end being closer to the hydrophobic medium,38 potentially contributing to the electric double layer. The water radical cation has been directly observed as the ionized water dimer $(H_2O)_2^{+\bullet}$ in microdroplets by Cooks and colleagues.[18] The $[^{\bullet}OH\cdots H_3O^+]$ structure, a conformation of $(H_2O)_2^{+\bullet}$, facilitates proton transfer and hydroxyl radical chemistry with appropriate substrates.[33] Our group has also prepared $(H_2O)_2^{+\bullet}$ ions *via* low-energy corona discharge ionization MS and investigated their interaction with DMA. The experimental setup is depicted in Fig. S18,† where one channel generates $(H_2O)_2^{+\bullet}$ ions while another channel produces DMA molecules. The results show a base peak at *m*/*z* 122 $(DMA + H)^+$ and a smaller peak at *m*/*z* 138 (*N*-hydroxyl-*N*,*N*-dimethylanilinium) as seen in Fig. S19.† Additionally, extracted ion chromatogram data indicate an increase in the ion intensity of the peak at *m*/*z* 138 after introducing DMA samples, while the intensity of the peak at *m*/*z* 36 decreases (Fig. S20†). These results suggest that $^{\bullet}OH$ radicals generated from $[^{\bullet}OH\cdots H_3O^+]$ by corona discharge MS are responsible for *N*-hydroxyl-*N*,*N*-dimethylanilinium (*m*/*z* 138) formation. In our study, high intensities of $(H_2O)_2^{+\bullet}$ ions and $DMA^{+\bullet}$ were also obtained at the gas–liquid interface of microdroplets under the influence of a strong electric field ($\sim 10^9$ V m^{-1}), as shown in Fig. 4b. At the gas–liquid interface, water dimer radical cations exist in the form of $[^{\bullet}OH\cdots H_3O^+]$ couples, with the $^{\bullet}OH$ radical being closer to the hydrophobic medium $DMA^{+\bullet}$, while the H_3O^+ end, being positively charged, is repelled by $DMA^{+\bullet}$ and moves away. Thus, *N*-hydroxyl-*N*,*N*-dimethylanilinium at *m*/*z* 138 is observed during DMA spraying.

The regional selectivity observed in our study aligns with the reactions of aromatic radical cations with nucleophiles and is supported by the single occupied molecular orbital (SOMO) distribution of $DMA^{+\bullet}$. As depicted in Fig. 4c, the SOMO of $DMA^{+\bullet}$ is significantly concentrated at the nitrogen atom site, as well as at the *ortho* and *para* positions relative to the *N*,*N*-dimethyl group. This distribution aligns with the experimental findings where *m*/*z* 138 corresponds to *N*-hydroxyl-*N*,*N*-dimethylanilinium. The cyclic voltammetry (CV) results for compounds **1–6**, shown in Fig. 4d, reveal relatively low oxidation peak potentials (1.1 V for DMA, 0.9 V for 4-OMe-DMA, 0.5 V for 4-Me-DMA, 0.9 V for 4-Cl-DMA, 1.0 V for 4-Br-DMA, 1.1 V for DMA, and 0.8 V for DEA), indicating their readiness to be oxidized at the anode. Together, the mechanisms for *N*-hydroxylation of DMA, derived from the intermediates captured by MS and the products from the scale-up synthesis, are summarized in Fig. 4e. Initially, DMA is spontaneously oxidized at the gas–liquid interface of water microdroplets, yielding the $DMA^{+\bullet}$ radical cation at *m*/*z* 121. This cation then reacts with the $^{\bullet}OH$ from the water dimer radical cation, with the $[^{\bullet}OH\cdots H_3O^+]$ structure, to produce *N*-hydroxyl-*N*,*N*-dimethylanilinium. This intermediate can further react to form *N*-hydroxyl-*N*,*N*-dimethylaniline *N*-oxide under certain conditions.

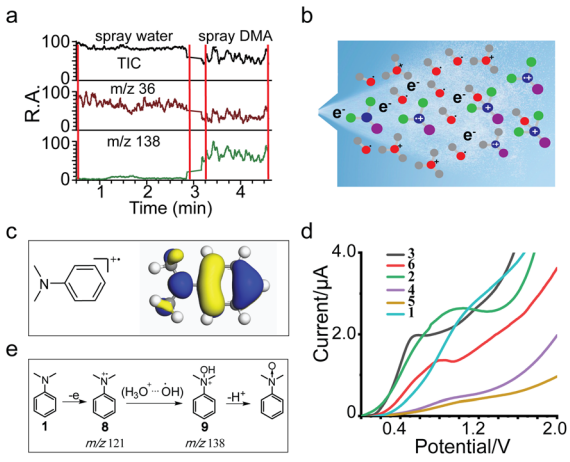

Fig. 4 Mechanistic studies and proposal. (a) Typical total ion chromatogram (TIC) and extracted ion chromatogram (EIC) showing reactants at *m*/*z* 36 and products at *m*/*z* 138 before and after spraying the DMA solution in microdroplets. (b) Schematic for the formation of *N*-hydroxyl-*N*,*N*-dimethylanilinium in microdroplets. (c) Computation of the singly occupied molecular orbital of the DMA radical cation at the B3LYP level of theory. (d) Cyclic voltammograms obtained in H_2O. **1**: DMA, **2**: 4-OMe-DMA, **3**: 4-Me-DMA, **4**: 4-Cl-DMA, **5**: 4-Br-DMA, and **6**: DEA. (e) Mechanistic proposal. DMA : *N*,*N*-dimethylaniline.

Conclusions

In summary, we have developed a green and rapid method for achieving *N*-hydroxylation of aromatic amines with diverse electronic properties, without the use of any catalysts or chemical oxidants. The intrinsic oxidation properties of water microdroplets are demonstrated by the generation of water dimer radical cations. Importantly, the *N*-hydroxylation of aromatic amines to quaternary ammonium cations was observed in water microdroplets. This result supports the idea that the strong electric fields within water microdroplets help aromatic amines lose one electron to form the corresponding

radical cations, which quickly capture the ˙OH radical generated from the dissociation of water radical cations to form quaternary ammonium cations. From this work, we anticipate that $(H_2O)_2^{+\bullet}$ will open a wide range of opportunities for designing new chemical reactions.

Data availability

Experimental data have been made available as the ESI. The authors declare that all the data that support the findings of the study are included in the main text and ESI.† The source data are available from the corresponding authors on request.

Author contributions

Xiaoping Zhang and Huanwen Chen identified and characterized the reactions and designed the experiments. Pinghua Hua and Minmin Duana performed the experiments and analyzed the experimental results. Xiaoping Zhang and Xinglei Zhang co-wrote the manuscript. Konstantin Chingin and Roman Balabin performed the computation and described the computational section.

Conflicts of interest

The authors declare that they have no competing interests.

Acknowledgements

This work was supported by the National Natural Science Foundation of China (22104014, 22364002, 22376084, and 22164002), Jiangxi Provincial Natural Science Foundation (20232BAB213047 and 20242BAB25138), Jiangxi Province International Cooperation Project (20203BDH80W010 and 20232BBH80012), The Youth Talent Support Program of Jiangxi Association for Science and Technology (2025QT06), and Jiangxi University of Chinese Medicine School-level Science and Technology Innovation Team Development Program (CXTD22005 and 2004-5252300403).

References

1 Z. Li, *et al.*, A tautomeric ligand enables directed C-H hydroxylation with molecular oxygen, *Science*, 2021, **372**, 1452–1457.
2 H. Long, T.-S. Chen, J. Song, S. Zhu and H.-C. Xu, Electrochemical aromatic C–H hydroxylation in continuous flow, *Nat. Commun.*, 2022, **13**, 3945.
3 J. Lv, B. Zhao, Y. Yuan, Y. Han and Z. Shi, Boron-mediated directed aromatic C–H hydroxylation, *Nat. Commun.*, 2020, **11**, 1316.
4 T. Baumeister, *et al.*, Continuous flow synthesis of amine oxides by oxidation of tertiary amines, *React. Chem. Eng.*, 2019, **4**, 1270–1276.
5 Y. Ogata, K. Tomizawa and H. Maeda, Kinetics of the tungstate-catalyzed H_2O_2 oxidation of amines in aqueous methanol. Acidity effect, *Bull. Chem. Soc. Jpn.*, 1980, **53**, 285–286.
6 M. P. Walsh, J. M. Phelps, M. E. Lennon, D. S. Yufit and M. O. Kitching, Enantioselective synthesis of ammonium cations, *Nature*, 2021, **597**, 70–76.
7 W. Wang, A. Buchholz, I. I. Ivanova, J. Weitkamp and M. Hunger, Synthesis and immobilization of quaternary ammonium cations in acidic zeolites, *Chem. Commun.*, 2003, 2600–2601.
8 C.-Y. Liu, Y. Chen and J. Hu, Identification of the electrogenerated hidden nitrenium ions by *in situ* mass spectrometry, *Anal. Chem.*, 2024, **96**, 3354–3361.
9 Q.-Y. Cheng, T. Wang, J. Hu, H.-Y. Chen and J.-J. Xu, *In situ* probing the short-lived intermediates in visible-light heterogeneous photocatalysis by mass spectrometry, *Anal. Chem.*, 2023, **95**, 14150–14157.
10 Q. Wan, *et al.*, Visible-light-activated aziridination reaction enables simultaneous resolving of C=C bond location and the sn-position isomers in lipids, *Chin. Chem. Lett.*, 2024, **35**, 108775.
11 X. Yan, Emerging microdroplet chemistry for synthesis and analysis, *Int. J. Mass Spectrom.*, 2021, **468**, 116639.
12 X. Yan, Y.-H. Lai and R. N. Zare, Preparative microdroplet synthesis of carboxylic acids from aerobic oxidation of aldehydes, *Chem. Sci.*, 2018, **9**, 5207–5211.
13 L. Zhao, *et al.*, Sprayed water microdroplets containing dissolved pyridine spontaneously generate pyridyl anions, *Proc. Natl. Acad. Sci. U. S. A.*, 2022, **119**, e2200991119.
14 H. Hao, I. Leven and T. Head-Gordon, Can electric fields drive chemistry for an aqueous microdroplet?, *Nat. Commun.*, 2022, **13**, 280.
15 M. T. C. Martins-Costa and M. F. Ruiz-López, Electrostatics and chemical reactivity at the air–water interface, *J. Am. Chem. Soc.*, 2023, **145**, 1400–1406.
16 J. K. Lee, *et al.*, Spontaneous generation of hydrogen peroxide from aqueous microdroplets, *Proc. Natl. Acad. Sci. U. S. A.*, 2019, **116**, 19294–19298.
17 C. Gong, *et al.*, Spontaneous reduction-induced degradation of viologen compounds in water microdroplets and its inhibition by host–guest complexation, *J. Am. Chem. Soc.*, 2022, **144**, 3510–3516.
18 L. Qiu and R. G. Cooks, Simultaneous and spontaneous oxidation and reduction in microdroplets by the water radical cation/anion pair, *Angew. Chem., Int. Ed.*, 2022, **61**, e202210765.
19 L. Qiu, M. D. Psimos and R. G. Cooks, Spontaneous oxidation of aromatic sulfones to sulfonic acids in microdroplets, *J. Am. Soc. Mass Spectrom.*, 2022, **33**, 1362–1367.
20 X. Zhang, *et al.*, Mass spectrometry distinguishing C=C location and cis/trans isomers: a strategy initiated by water radical cations, *Anal. Chim. Acta*, 2020, **1139**, 146–154.
21 W. Yang, *et al.*, Determination of C=C positions of unsaturated fatty acids in foods *via* ambient reactive desorption ionization with water dimer radical cations, *J. Agric. Food Chem.*, 2024, **72**, 845–856.

22 X. Zhang, X. Ren, Y. Zhong, K. Chingin and H. Chen, Rapid and sensitive detection of acetone in exhaled breath through the ambient reaction with water radical cations, *Analyst*, 2021, **146**, 5037–5044.
23 X. Zhang, *et al.*, Efficient catalyst-free N_2 fixation by water radical cations under ambient conditions, *Nat. Commun.*, 2024, **15**, 1535.
24 P.-R. Pan, Y.-S. Lin, M.-K. Tsai, J.-L. Kuo and J.-D. Chai, Assessment of density functional approximations for the hemibonded structure of the water dimer radical cation, *Phys. Chem. Chem. Phys.*, 2012, **14**, 10705–10712.
25 Q. Wan, *et al.*, Elucidating the underlying reactivities of alternating current electrosynthesis by time-resolved mapping of short-lived reactive intermediates, *Angew. Chem., Int. Ed.*, 2023, **135**, e202306460.
26 T. A. Brown, H. Chen and R. N. Zare, Detection of the short-lived radical cation intermediate in the electrooxidation of *N*,*N*-dimethylaniline by mass spectrometry, *Angew. Chem., Int. Ed.*, 2015, **127**, 11335–11337.
27 T. Morofuji, A. Shimizu and J.-i. Yoshida, Direct C–N coupling of imidazoles with aromatic and benzylic compounds *via* electrooxidative C–H functionalization, *J. Am. Chem. Soc.*, 2014, **136**, 4496–4499.
28 T. Morofuji, A. Shimizu and J.-i. Yoshida, Electrochemical C–H amination: synthesis of aromatic primary amines *via* *N*-arylpyridinium ions, *J. Am. Chem. Soc.*, 2013, **135**, 5000–5003.
29 J. K. Lee, S. Kim, H. G. Nam and R. N. Zare, Microdroplet fusion mass spectrometry for fast reaction kinetics, *Proc. Natl. Acad. Sci. U. S. A.*, 2015, **112**, 3898–3903.
30 M. Girod, E. Moyano, D. I. Campbell and R. G. Cooks, Accelerated bimolecular reactions in microdroplets studied by desorption electrospray ionization mass spectrometry, *Chem. Sci.*, 2011, **2**, 501–510.
31 W. Yang, Q. Qi, W. Liu, M. Li and Y. Luo, Synthesis of isotope-labeled ^{15}N-*N*,*N*-dimethylaniline, *Chin. J. Org. Chem.*, 2012, **32**, 145–148.
32 D. Xing, *et al.*, Capture of hydroxyl radicals by hydronium cations in water microdroplets, *Angew. Chem., Int. Ed.*, 2022, **61**, e202207587.
33 M. Wang, *et al.*, Abundant production of reactive water radical cations under ambient conditions, *CCS Chem.*, 2022, **4**, 1224–1231.
34 D. Mi, *et al.*, Generation of phenol and molecular hydrogen through catalyst-free C-H activation of benzene by water radical cations, *J. Am. Soc. Mass Spectrom.*, 2022, **33**, 68–73.
35 M. Zheng, X. Zhang, Y. Cheng, L. Sun and X. Zhang, Hydroxyl transfer *versus* cyclization reaction in the gas phase: sequential loss of NH_3 and CH_2CO from protonated phenylalanine derivatives, *Front. Chem.*, 2023, **10**, 1094329.
36 X. Zhang, *et al.*, Demethylation C–C coupling reaction facilitated by the repulsive Coulomb force between two cations, *Nat. Commun.*, 2024, **15**, 5881.
37 H. Cheng, S. Tang, T. Yang, S. Xu and X. Yan, Accelerating electrochemical reactions in a voltage-controlled interfacial microreactor, *Angew. Chem., Int. Ed.*, 2020, **59**, 19862–19867.
38 S. Pullanchery, S. Kulik, B. Rehl, A. Hassanali and S. Roke, Charge transfer across C–H···O hydrogen bonds stabilizes oil droplets in water, *Science*, 2021, **374**, 1366–1370.